Correspondences between parameters in a reaction-diffusion model and connexin functions during zebrafish stripe formation

Akiko Nakamasu (nakamasu@kumamoto-u.ac.jp)
Kumamoto Univ.

Article

Keywords: Pattern formation, Turing pattern, mathematical model, Reaction-diffusion system

Posted Date: June 29th, 2021

DOI: https://doi.org/10.21203/rs.3.rs-658862/v1

Title; Correspondences between parameters in a reaction-diffusion model and connexin functions during zebrafish stripe formation.

Akiko Nakamasu*

International Research Organization for Advanced Science and Technologies, Kumamoto University, 2-39-1 Kurokami, Chuo-Ku, Kumamoto, 860-8555 Japan

* Corresponding author

Email: nakamasu@kumamoto-u.ac.jp

Keywords

Pattern formation, Turing pattern, mathematical model, Reaction-diffusion system.

Abstract

Different diffusivities among interacting substances actualize the potential instability of a system. When these elicited instabilities manifested as forms of spatial periodicity, they are called Turing patterns. Simulations using general reaction-diffusion (RD) models have demonstrated that pigment patterns on the body trunk of growing fish follow a Turing pattern. Laser ablation experiments performed on zebrafish revealed apparent interactions among pigment cells, which allowed for a three-components RD model to be derived. However, the underlying molecular mechanisms responsible for Turing pattern formation in this system had been remained unknown. A zebrafish mutant with a spotted pattern was found to have a defect in Connexin41.8 (Cx41.8) which, together with Cx39.4, exists in pigment cells and controls pattern formations. Here, molecular-level evidence derived from connexin analyses was linked to the interactions among pigment cells described in previous RD modeling. Channels on pigment cells were generalized as “gates,” and the effects of respective gates were deduced. The model used partial differential equations (PDEs) to enable numerical and mathematical analyses of characteristics observed in the experiments. Furthermore, the improved PDE model included nonlinear reaction terms, enabled the consideration of the behavior of components.

Introduction

In 1952, Alan Turing postulated that two substrates interacting with each other show instability when they diffuse at different speeds. He explained this diffusion-driven instability by utilizing a linear reaction-diffusion (RD) model. This model demonstrated that spatial inhomogeneity (i.e., Turing pattern) could be generated by such conditions (Turing, 1952). This relationship is known to generate patterns, though the components remain to be explored.

More than two decades ago, Kondo and Asai (1995) reported that pigment stripes on the bodies of growing marine angel fish behaved as a Turing pattern. Research focus then shifted mainly to zebrafish (*Danio rerio*) as a model organism for pattern formation studies (Johnson *et al.*, 1995a, b; Kelsh, 2004). Zebrafish have a pattern of stripes on their body and fins (Fig. 1A). The pattern is generated by three types of pigment cells: complementarily distributed black melanophores and yellow xanthophores (Fig. 1C), plus iridescent iridophores. Numerous zebrafish pigment-pattern mutants were artificially generated (Haffter *et al.*, 1996) and the corresponding genes were identified. One of the most important mutants is *leopard*, which produce a spotted pattern, that is representative of Turing patterns (Fig. 1B). Watanabe *et al.* (2006) identified *connexin41.8* (*cx41.8*) as the gene responsible for the *leopard* mutation. Besides Cx41.8, other connexins such as Cx39.4 exist in pigment cells and affect pigment-pattern formation. Six connexins form a hemi-channel (or “connexon”), which connects intracellular and extracellular spaces (Fig. 1D). Docking of two hemi-channels from adjacent cells give rise to a gap junction, which mediates intercellular signal transfer (Kumar and Gilula, 1996). The minimal connexin network required to originate a striped pattern was recently revealed by regulating connexin expression in each pigment cell (Usui *et al.*, 2019). Therefore, these channels are important for pigment-pattern formation.

Interactions among pigment cells and their molecular mechanisms involved in pattern formation are summarized in Volkening (2020). However, the molecular mechanisms leading to Turing instability have remain mostly unresolved. Mosaic fish experiments have indicated that both *leopard/cx41.8* and *jaguar/obelix/kcnj13* genes are required for segregation of melanophores and xanthophores. Such segregation was proposed to involve local interactions between adjacent pigment cells (Maderspacher and Nusslein-Volhard, 2003). Xanthophore ablation using a temperature-sensitive *csf1ra* allele led to the gradual death of melanophores in both the body trunk and fins of adult fish (Parichy and Turner, 2003). Accordingly, melanophore survival requires continuous signaling from xanthophores. Laser ablation of stripe and inter-stripe areas has revealed the mutual interactions between melanophores and xanthophores (Nakamasu *et al.*, 2009). The interactions comply with the requirements for Turing pattern formation (Fig. 1E). Specifically, both types of pigment cells activate their own type at a single-

cell distance (short range) by mutual inhibitions of other types, but then inhibit their own type beyond the width of the stripe (long range). The difference in reaction distances achieves the "local activation and lateral inhibition" condition needed for pattern formations (Meinhardt and Gierer, 1974). It should be noted, however, that the distinction between iridophores and xanthophores was sometimes unclear in those experiments.

To explain the opposing actions at long *vs*. short distance, a model that included a highly diffusible molecule (i.e., long-range factor) and two cells (regarded as short-range factors with low diffusivity) was constructed (Nakamasu *et al.*, 2009). This three-component RD model, with its linear reaction terms and upper and lower limits, described the apparent interactions obtained experimentally. Then the different diffusibilities and the interactions in the model achieved diffusion-driven instability (Turing instability).

Further investigations revealed that the interactions were mediated by cell projections (Hamada *et al.*, 2014). The interaction mediated by gap junctions on the tip of the projection was considered to be a long-range effect observed in the previous experiments (Watanabe and Kondo*,* 2015). The researchers mentioned the possibility that the pattern formation might not require actual diffusion. Later a Turing model based on an integral kernel was suggested (Kondo, 2017), though the link between parameter and molecular function was ambiguous. Most other models for the pigment-pattern formation are based on interactions at a cellular level. These models implemented different effects depending on the distance from each pigment cell (Bullara and De Decker, 2015; Volkening and Sandstede, 2018; Owen *et al.,* 2020). Several attempts were made to explain the observed patterns in zebrafish mutants by a general Turing model (Asai *et al.*, 1999; Watanabe and Kondo, 2012); however, they were not supported experimentally, even though there are several paths to cause the expected pattern changes in mutants.

Here, the interactions in a three-component model, including a highly diffusible factor, were developed to attempt to link the molecular functions of connexins in zebrafish. Channels thought to be important for the pattern formation were generalized as "gates" of pigment cells. These gates enable transport of the diffusible molecule across the membrane. The parameters affected by each gate were deduced, then the effects on pattern-selection and -size, were analyzed. Finally, the model was improved to an analogous model with nonlinear terms. These models together enabled reasonable explanations of detailed behavior of the components that related to the pattern formation.

Results

Linear reaction-diffusion model for pigment-pattern formation

Previous laser ablation experiments revealed that the presence of mutual interactions between two types of pigment cells were necessary to generate Turing patterns (Fig. 1E). A mathematical model was derived from these apparent interactions in Nakamasu *et al.* (2009), although the details of the relationship between the experimental results and the model were not described. This model was based on the following set of RD equations:

$$\begin{cases} \dfrac{\partial u}{\partial t} = D_u \nabla^2 u + f(v,w) - d_u u \\ \dfrac{\partial v}{\partial t} = D_v \nabla^2 v + g(u,w) - d_v v \\ \dfrac{\partial w}{\partial t} = D_w \nabla^2 w + h(u,v) - d_w w \end{cases} \quad (1)$$

Here the alternative distribution of two types of pigment cells (Fig. 1C) was expressed by two factors (U, V) of the three components. Then u, and v was each volume. Numerical simulation of this model resulted in a Turing pattern in which u and v were distributed with antiphase while a concentration of third factor W (w), presented peaks synchronized with u (Fig. S1). It should be noted that cell divisions of differentiated melanophores contribute only minimally to the pigment-pattern formation in fish (Fig. 1F). Therefore, the number of melanophores is changed by 1) supply of new cells from randomly scattered precursor cells, 2) death of existing pigment cells, or 3) migration from a position close to the skin surface (Takahashi and Kondo, 2009). In the case of melanophores, it is known that cell movements and cell deaths are complementary to each other (Sawada *et al.*, 2018). Even though they are inhibited, xanthophores are found in the stripe region, where they exist with a pale color (Hirata *et al.*, 2003, 2005; Mahalwar *et al.*, 2014). Xanthophores do not move actively *in vivo*, as may be the case for iridophores. As detailed in Fig. 1F, motilities of the cells were approximated by small diffusion coefficients (D_u and D_v). The rapidly diffusing factor W was assigned a large diffusion coefficient (D_w).

The parameters in the reaction formulae were positive constants as shown in Table 1. Each formula was composed of a set of linear terms with upper and lower limits as follows:

$$\begin{cases} f(v,w) = \begin{pmatrix} 0;\ -i_{uv}v - i_{uw}w + s_u < 0 \\ -i_{uv}v - i_{uw}w + s_u;\ 0 < -i_{uv}v - i_{uw}w + s_u < f_{max} \\ f_{max};\ -i_{uv}v - i_{uw}w + s_u > l_{max} \end{pmatrix} \\ g(u,w) = \begin{pmatrix} 0;\ -i_{vu}u + p_{vw}w + s_v < 0 \\ -i_{vu}u + p_{vw}w + s_v;\ 0 < -i_{vu}u + p_{vw}w + s_v < g_{max} \\ g_{max};\ -i_{vu}u + p_{vw}w + s_v > m_{max} \end{pmatrix} \\ h(u,v) = \begin{pmatrix} 0;\ p_{wu}u - c_{wv}v + s_w < 0 \\ p_{wu}u - c_{wv}v + s_w;\ 0 < p_{wu}u - c_{wv}v + s_w < h_{max} \\ h_{max}; p_{wu}u - c_{wv}v + s_w > n_{max} \end{pmatrix} \end{cases} \quad (2)$$

The cells were assumed to be inhibiting mutually ($-i_{uv},\ -i_{vu}$), then W was assumed to be produced by U (p_{wu}) and consumed by V ($-c_{wv}$). Accordingly, W was assumed to inhibit pigment cells of the producer ($-i_{uw}$) and produce (or preserve) the consumer (p_{vw}). The self-coupling parameters $-d_u,\ -d_v,\ -d_w$ corresponded to degradation (or death) coefficients, whereas s represented constants related to supply (also called "support sustainability") of each component. The producer U activated V, but then inhibited itself at long range via W. By consuming W, V also indirectly inhibited itself, but then was activating U by double inhibition at long range. As a result, U and V exhibited no difference in apparent interactions, making it difficult to identify which factor corresponded to which cell type. Besides melanophores, xanthophores also showed self-inhibition at long range. In laser ablation experiments, melanophore elimination in adjacent stripes caused pale-colored xanthophores in an inter-stripe region. Therefore, the pale color reflects xanthophore inhibition even without a change in cell number.

The three-component model in (1) is somewhat complex, though it can be applied to a combination of two-variable systems as follows.

$$\begin{cases} \dfrac{\partial x}{\partial t} = f_x\, x + f_y\, y + D_x \nabla^2 x \\ \dfrac{\partial y}{\partial t} = g_x\, x + g_y\, y + D_y \nabla^2 y \end{cases} \quad (3)$$

There are two different cases that bring diffusion driven instabilities, i.e., activator-inhibitor type (Fig. 2A) or activator-substrate-depletion type (Fig. 2B), characterized by different signs of the parameters (Gierer and Meinhardt, 1972, Murray, 1989). Both conditions were included in the three-component model (Fig. 2C). Therefore, each parameter in the model can be regarded as part of a two-variable system. The first and second reaction formulae (2) include mutual inhibitions ($-i_{uv}v,\ -i_{vu}u$), each of which corresponds to the respective self-activation ($f_x > 0$ for x), though it cannot be realized without each partner. Recent experiments revealed that xanthophores are generated from division of other xanthophores (Mahalwar *et al.*, 2014).

Therefore, at least one of self-reaction parameters; $-d$ for u or v in (2), cannot be a degradation coefficient, i.e., it might be a non-negative parameter.

Effects of the parameters on the component proportion and the characteristic wavelength of a pattern.

Variation in patterns observed in most zebrafish mutants is explained by changes in the types and sizes of patterns. The former is defined by pattern selection (Ermentrout, 1991, Shouji *et al.*, 2003), and manifests as a general variation of the Turing pattern from spots, to stripes to reverse spots. The latter is dictated by the characteristic wavelength of the pattern (Miura and Maini, 2004). The following sections analytically describe the effect of parameters in the model (1)-(2) on these characteristics.

Effects of parameter on pattern size

The characteristic wavelength of a pattern can be analytically derived from the dispersion relation of linear stability (Miura and Maini, 2004). The wavelength of a two-variable RD system (3) is given by the following equations:

$$\frac{2\pi}{k_{max}} = \sqrt{\frac{\sqrt{D_x D_y}\left(D_y - D_x\right)}{\left(D_x + D_y\right)\sqrt{-f_y g_x} - \sqrt{D_x D_y}\left(f_x - g_y\right)}} \tag{4}$$

k_{max} is a preferable wave number in a system. As mentioned above, each parameter in the model can be regarded as a two-variable system (Fig. 2C). The mutual inhibitions ($-i_{uv}v$, $-i_{vu}u$) correspond to the self-activation, though they are inversely related, i.e., the sign of the parameters is different from f_x in two-variable systems. The increase in the absolute values of the parameters reinforces the self-activation. At the same time, the effects of $-d_u$ and $-d_v$ are opposite of f_x. The effect on pattern size when the absolute value of each parameter is decreased (i.e., the decline of each interaction) is shown in Fig. 2D and indicates correspondence with two-variable systems (Fig. 2A, B).

Effects of parameter on pattern selection

In zebrafish, pattern selection is determined mainly by the proportion of two types of pigment cells with complimentary distribution. The relative position of the equilibrium from the limits of the reaction terms provides an index for pattern selection (Shouji *et al.*, 2003), as that is the origin of diffusion-driven instability.

Considering differential equations of the volume of two cells (u and v), the decrease in each absolute value (i.e., the decline of each interaction) of the parameter with a positive effect decreases the population volume of respective cells, then that of the parameter with a negative effect increase the population of the respective cells. Here, the component W with high diffusivity represses u and promotes v, therefore, the decrease in the positive parameter in the differential equations of w increases u and decreases v respectively. The opposite can apply to negative parameters. From this aspect, however, it is difficult to refer about the combined effect of parameters with different signs.

Correspondence between the mathematical model and connexin defects in zebrafish estimated from molecular function

Next, correspondence between this model and molecular functions was assumed (Fig. 1G). In zebrafish, *leopard* mutants are known to have an aberrant pigment pattern, whereby stripes are changed to spots (Watanabe *et al.*, 2006) (Fig. 1A, B). The gene responsible for the *leopard* mutation is a connexin *cx41.8*, which encodes a four trans-membrane connexin protein. Additionally, mutation of connexin *cx39.4* results in wavy stripes. Recent analyses of connexin activity have revealed different functions associated with hemi-channels and gap junctions (Misu *et al.*, 2016, Watanabe *et al.*, 2016). Hemi-channels are open to the extracellular environment, whereas gap junctions form connections between cells to allow the exchange of small molecules (Fig. 1D). Accordingly, connexins may be involved in both long- and short-range interactions. These channels may function as gates for the transport of molecule W across the membrane (Fig. 1G). Accordingly, producer U produces W, which then diffuses outside the cell into the extracellular space via some kind of gate. Therefore, gate defects affect survival of the producer by preventing release of harmful W (i. e., d_u of $-d_u$ is increased). I considered two other possibilities, i.e., the effect of gate defect on D_w and/or i_{uw}. If D_w was changed, W outside of the cells will also be affected. A u-dependent decrease in D_w might be more appropriate for the assumption of enclosed W. Though, it will give difficulties in the analytical approach and both will finally result in an increase in the degradation of U. Then the concentration of W that gave the same effect on U would not change. Therefore, D_w and i_{uw} would not be affected. w had peaks with the peaks of producer U and the gates on cells assumed passive effects on W movements. This explain why p_{wu} might not be affected, at least directly. Consumer V was assumed to incorporate beneficial W into the cell across the gates then to consumes it, indicating that the gate defects will decrease the parameters c_{vw} of $-c_{vw}$ and p_{wv}. Both parameters were assumed to be related to intracellular events, therefore, higher w was needed for the same rate of consumption and V production compared with the

case of intact hemi-channels. At the same time, parameters for mutual inhibitions i_{uv} and i_{vu} are decreased by the *leopard* mutation (Yamanaka and Kondo, 2013) through gap junctions (combination of gates) at short range. They would be simultaneously affected linking with the hemi-channel defect on the corresponding cell. In Fig.1G, these parameters linked to different gates are indicated by different hatchings.

Comparisons of results obtained by simulation and experiments.

First, the independent effects of the gate on each cell were analyzed numerically. When an arbitrary stripe is set as a starting point, only gates that opened to the outside on U and V cells were removed along the x- and y-axes. Numerical simulation of this model yielded a spot pattern of u in the case where gates on U cells had defects, as expected by the sing of the parameter (Fig. 3A). Reversed u spots were yielded in V cell defects (Fig. 3B), though the change was not strong, because it included opposite effects on V volume. Pattern simplicity score (PSS) increased in both cases, then overall color tones (OCT) were decreased and increased by respective defects. That is, the asymmetry of changes in pattern selection can be observed by the removals of gates on respective cell types.

The results mostly consisted with the positive effects of connexin additions to WKO that increased the respective pigment cells (Usui *et al.*, 2019). However, experimental eliminations of gate on each wild-type pigment cell led to an increase in the rate of respective pigment cells; melanophore defects generated net patterns of melanophores, while the xanthophore defects resulted in dot patterns of melanophores (i.e., net patterns of xanthophore).Therefore, the simulation results were partly inconsistent with experimental results in Usui *et al.* (2019), in which the effects of connexins on each or both pigment cells were investigated in detail (Fig. 3K).

Defects on short-range inhibition did not have drastic effects on pattern selection, though the pattern did finally disappear (Fig. 3C). On the 2D plane, the stripe region was recessive together with the defect in short-range effects by gap-junctions (Fig. 3D-H, J), though the tendency to shift the pattern selection was not changed. In Fig. 3I, short-range effects were simultaneously decreased by respective x or y values that linked with U or V defects, as shown in right panel in Fig. 3J. This also kept the same tendency to shift the pattern selection with individual cases. From the electro-physiological experiments in Watanabe *et al.* (2016), each type of connexin could be considered to have different strengths of the (hemi-) channel functions on the two types of cells. Deduced patterns of respective transgenic fishes were

indicated by small letters on the phase plane in Fig. 3I. Even though the differences in the strengths of channels were taken account, the removal of hemi-channels on wild-type xanthophores tended to increase the population of xanthophore then a faint increase in melanophores was brought in the case of connexin on melanophores (Fig. 3K). If cell U is a melanophore, other than the gray-framed patterns shown in Fig. 3K did not seem to correspond to Fig 3I, though all of the experimentally obtained patterns are existed in the simulation. As describe more distinctly, some shuffles can give a strong correspondence with Fig. 3I (Fig. S2).

From the analyses mentioned above, defects to the gates on cell U (increasing in d_u of $-d_u$) or cell V (decreasing in p_{vw} and c_{wv}) caused a decrease or an increase in pattern size, respectively. In numerical simulations, the pattern size tended to be decreased and increased by the hemi-channel defects on both U and V cells, as expected (Fig. 3A, B). The characteristic thinning of u stripes and widening of v inter-stripes were observed by the U-cell defects, though it was not explained by the analyses. From the characteristic thinning of the u stripe, each cell corresponding to one of two short-range factors may be deduced. However, the thinning was observed on melanophore stripe, in the case of defect in xanthophore. Inconsistent with the U defect, melanophore defect tented to result in wide melanophore stripes.

Non-linearization of the model

To describe the behavior of the components in the system in greater detail, the model was non-linearized. As an example, we devised a model with nonlinear terms as shown in (5), though qualitative relationships were not changed from the model shown in Fig 1F.

$$\begin{cases} \dfrac{\partial u}{\partial t} = D_u\nabla^2 u - i_{uv}uv - i_{uw}uw + d_u u + \dfrac{s_u}{1+u+v} \\ \dfrac{\partial v}{\partial t} = D_v\nabla^2 v - i_{vu}vu + p_{vw}vw - d_v v + \dfrac{s_v}{1+u+v} \\ \dfrac{\partial w}{\partial t} = D_w\nabla^2 w + p_{wu}u - c_{wv}wv - d_w w + s_w \end{cases} \quad (5)$$

This model, using nonlinear RD equations, also generated Turing patterns. Considering interactions between different types of cells and between cells and molecules, inhibitions were given by multiplication terms (e.g., the inhibition of U by W was described as uw, and so on). These multiple terms are based on the description of second-order reaction in chemical kinetic equation or dimer reactions by Meinhardt (1982), it enabled only limited reaction by the contacts between the components. W was needed for maintenance of cell V so this reaction was also given by a multiplication term of their volume. On the other hand,

production of W by U will only occur u-dependently, and degradation (and deaths) will also be w-dependent. Therefore, those terms are linearly related to each component. These non-linearizations can identify the actions on an existing cell or a newly differentiating cell. Then new generations of pigment cells occur only with eliminations of existing cells (Yamaguchi *et al.* 2007). Therefore, mature cells would inhibit the generation of cells. The sign of d_u seemed prefer to be positive for the start point of pattern selection corresponded to zebrafish i.e., the start from stripe. Even though the sign was opposite to the linear model, total u change may become minus with relation to other components (i.e., $-i_{uv}v - i_{uw}w + d_u < 0$ in the deformed reaction terms $(-i_{uv}v - i_{uw}w + d_u)\, u + s_u/(1 + u + v)$). Therefore, the self-productivity can be small enough to agree with the low proliferation rate of melanophores. Similar, concerns about the self-productivity of xanthophores mentioned above, $\partial v/\partial t$ in (5) already had a self-productivity by the multiplication term vw, regardless of the sign of d_v (i.e., $-i_{vu}u + p_{vw}w - d_v > 0$ in deformed reaction terms $(-i_{vu}u + p_{vw}w - d_v)\, v + s_v/(1 + u + v)$). The sign of d_v can be inverted though the change were not expected to substantially affect pattern characteristics.

Next, numerical calculations of the nonlinear model were performed to consider the condition where respective gates on U and V cells, and both-gate defects were added (Fig. 4A-C). Again, numerical results consistent with linear model could be obtained from an arbitrary parameter set generating a stripe pattern. Biased pattern shift could also be obtained by simulations, partly corresponding to connexin-mutation experiments. When gates on U cell were deleted, it resulted in a u dot pattern (Fig. 4A). Simultaneous decreases in p_{vw} and c_{wv} by increasing the gate defect on V cells generated a net of u, though not so drastic (Fig. 4B). Defect in gap-junction by decreasing i_{vu} and i_{uv}, had minimal effect, though the stripe region became recessive with combination of defects on each outer gate (Fig. 4C, D). The thinning of the u population was not clear because of the thin stripe at the start.

Discussion

In the present study, to confirm the potency of diffusion-driven instability in determining fish pigmentation patterns, channels on pigment cells were generalized as “gates” (Fig. 1). The three-component RD model (1) was shown to be composed of two-variable RD systems bringing diffusion driven instabilities (Fig. 2). The proposed qualitative models help to understand the relationship between pigment cells, as well as between cells and molecules, even when their identity is unknown. The terms of the theoretical model were connected with the functions of each channel on different cells. Parameters affected by the gate defects were deduced (Fig.1G) then the effects of such defects were simulated from a parameter set that generated an arbitrary stripe as a benchmark (Fig. 3, 4). Then, dots and thinning of the U cell population could be obtained by a defect of the gate on it in numerical simulations. The identities of melanophores and xanthophores were deduced from the change of pattern selection and the wavelengths, though the identify of important substance W is still missing. Then, improvements to the nonlinear model enabled a description of the detailed behaviors of components that are related to the pattern formation. Though the numerical analyses could not strictly explain the pattern obtained by experimental manipulation of connexins by Usui *et al.* (2019), the present study can help to interpret the mechanism underlying the *leopard* mutation, as a Turing system.

The determinations of the signs of self-reaction terms for U and V were difficult. The signs of d_u prefer to invert for a desirable range of pattern selection start from stripe in the improved nonlinear model, though the total changes for U (= melanophore) corresponded to experimental observations. The increase in existing melanophores brought by positive d_u were visible by the laser ablation of adjacent xanthophores or deletion of stripes in the experiments in Nakamasu *et al.* (2009), Each manipulation decrease $-i_{uv}v$ or $-i_{uw}w$ inhibitions, respectively. On the other hand, the self-productivity of xanthophores in the nonlinear model can be achieved even though the negative coefficient of self-reaction. The combination of two-cases of diffusion driven instability in the three-component model indicates the capacity to make a pattern without melanophore by the self-productivity of xanthophore, if sufficient W is added externally. On the other hand, if melanophores have strong self-productivity, it will also be able to make a pattern without xanthophores by the removal of extra W.

Connexins are related to both hemi-channels and gap junctions. Hemi-channels have been considered less important in physiology, although it was recently revealed that the aberrant activity of hemi-channels could change the proportion of vertebrae (Misu *et al.*, 2016) and was related to the pigment-pattern formation in zebrafish (Watanabe *et al.*, 2016; Watanabe, 2017). Laser ablation experiments showed that the interactions between

xanthophores and melanophores differed depending on the distance. In the present model, the highly diffusible molecule W had a positive effect on V. Hence, the inhibition of V via gap junctions is inconsistent. Outflow of harmful W from U via gap junctions is also inconsistent with the inhibition. This elicits a different signal transduction cascade as cell depolarization (Inaba *et al.*, 2010) and incorporation of functions for molecules other than connexin should be envisioned. Then the inverted function may be derived from an observed rectified current in gap junction. It was observed that quail melanocytes interacted with each other via filopodia *in vivo* and *in vitro* (Inaba *et al.*, 2019). Gap junctions may have functions on interactions not only between other types of cells but among the same populations. Though, the obtained simulation results included several collisions with experimental results. Similar discords were also in experiments. The results of Usui *et al.* (2019) indicated that either Cx41.8 or Cx39.4 is needed on melanophores then Cx41.8 is necessary and sufficient on xanthophore for (stripe) pattern formation. However, such “necessary and sufficient” trait for aberrant currents could be observed in hemichannels composed of Cx39.4 in the absence of calcium, in electro-physiological experiments (Watanabe *et al.*, 2016). Shuffle of mutant fish further supported the numerical results shown in Fig. S2. In this case, expected Cx41.8 manipulations showed the “necessary and sufficient” trait on melanophores.

Similar effects of connexin mutations (i.e., shift from stripe to dots) can be observed both on the body and fins. Because of the fins lack iridophores, the effect on the pigment pattern formation depends on the relationship between melanophores and xanthophores. Even though pattern formation is achieved by the two types of cells, details on the role of iridophores in cellular interactions have been revealed (Maderspacher and Nusslein-Volhard, 2003). The evaluation of the iridophore function in similar modeling will also be possible and should be attempted.

Using such a model with partial differential equations will lead to various mathematical analyses. For example, pattern size was mathematically analyzed with regard the model as combination of two-variable systems here. This method cannot yet describe the independent pattern sizes of each type of pigment cell that have been observed experimentally (Watanabe & Kondo, 2012) and predicted numerically. Therefore, more sophisticated analyses will be required in the future.

Materials and Methods

Numerical simulations

For the linear model, d_u was increased from 0 to 0.2 within limits along the x-axis (Fig. 3A, D-H) and the parameters p_{vw} and c_{wv} were decreased linearly from 1 to 0 (Fig. 3B, D-H) for investigation of the effect of gates on each cell. For short-range effects, i_{uv} and i_{vu} were decreased linearly from 1 to 0.6 in Fig. 3C. Accordingly, the arbitrary parameter set generating stripes (wild-type) was placed in the right top of the phase plane (Fig. 3D-I). Partial differential equations were calculated with 20000 and 40000 iterations with $dt = 0.1$ and $dt = 0.05$, in fields sized $xl = 56.25,\ yl = 225$ with $dx = 0.75$ and $xl = yl = 200$ with $ds = 0.5$ for Fig. 3A-C and Fig. 3D-H, respectively. In Fig. 3I, to investigate the simultaneous gap-junction effects with hemi-channels $s_d(x, y) = 1 - 0.002\, max\{x, y\},\ u_d(x) = 0.0004x$, and $v_d(y) = 1 - 0.002y$ were utilized in the field sized $x = y = 300$ $(dx = 0.75)$ and $dt = 0.1$ for 20000 iterations.

For the non-linear model, the parameters d_u, and i_{uv} and i_{vu} were decreased linearly from 1 to 0.6. c_{wv} and p_{vw} were decreased linearly from 0.5 to 0.1 in Fig. 4 A-C, and decreased by $s_d(x, y) = 1 - 0.002\, max\{x, y\}$ simultaneously in Fig. 4D. Accordingly, the arbitrary parameter set generating stripes (wild-type) was placed in the right top of the phase plane. Partial differential equations were calculated in fields sized $xl = 10,\ yl = 40$ in Fig. 4A-C and $xl = yl = 50$ with $ds = 0.25$ in Fig. 4D. Then after 500000 iterations calculated with $dt = 0.01$, we obtained the result.

Calculations were performed in the language Full BASIC with no-diffusion boundary conditions then and results are shown as density plots of u. Parameters utilized in this study are summarized in Table 1.

Quantification of color patterns

Color pattern complexity and overall tone were quantified from binarized images using the ImageJ as described in Miyazawa *et al.* (2010). Briefly, the pattern simplicity score (PSS) is defined as the area weighted mean isoperimetric quotient of the contours extracted from each image. The overall color tone (OCT) of a pattern is defined and calculated as the ratio of white pixels in the binarized image. Analyzed images were prepared by the quaternary connection of a numerical result (100×100 individual fields with periodic boundary conditions) of u in each parameter.

References

1. Turing, A. M., (1952). The chemical basis of morphogenesis. *Philos. Trans. R. Soc. Lond. B* **462**, 27-73.
2. Kondo, S. and Asai, R., (1995). A reaction-diffusion wave on the skin of the marine angelfish Pomacanthus. *NATURE* **376**, 765-768.
3. Johnson, S. L., Africa, D., Horne, S. and Postlethwait, J. H., (1995a). Half-tetrad analysis in zebrafish: Mapping the ros mutation and the centromere of linkage group I. *Genetics* **139**, 1727-1735.
4. Johnson, S. L., Africa, D., Walker, C. and Weston, J. A., (1995b). Genetic control of adult pigment stripe development in zebrafish. *Dev. Biol.* **167**, 27–33.
5. Kelsh, R. N., (2004). Genetics and evolution of pigment patterns in fish. *Pigment Cell Res.* **17**, 326-336.
6. Haffter, P., Granato, M., Brand, M., Mullins, M. C., Hammerschmidt, M., Kane, D., Odenthal, J., van Eeden, F. J., Jiang, Y. J., Heisenberg, C. P., Kelsh, R. N., Furutani-Seiki, M., Vogelsang, E., Beuchle, D., Schach, U., Fabian, C. and Nüsslein-Volhard, C., (1996). The identification of genes with unique and essential functions in the development of the zebrafish, *Danio rerio*. *Development* **123**, 1-36.
7. Watanabe, M., Iwashita, M., Ishii, M., Kurachi, Y., Kawakami, A., Kondo, S. and Okada, N., (2006). Spot pattern of *leopard* Danio is caused by mutation in the zebrafish connexin41.8 gene. *EMBO reports* **7**, 893-897.
8. Kumar, N. M. and Gilula, N. B., (1996). The gap junction communication channel. *Cell* **84**, 381-388.
9. Usui, Y., Aramaki, T., Kondo, S. and Watanabe, M., (2019). The minimal gap-junction network among melanophores and xanthophores required for stripe-pattern formation in zebrafish. *Development* **146**, dev181065.
10. Volkening, A., (2020). Linking genotype, cell behavior, and phenotype: multidisciplinary perspectives with a basis in zebrafish patterns. *Curr. Opin. Genet. Dev.* **63**, 78-85.
11. Maderspacher, F. and Nusslein-Volhard, C., (2003). Formation of the adult pigment pattern in zebrafish requires *leopard* and *obelix* dependent cell interactions. *Development* **130**, 3447-3457.
12. Parichy, D. and Turner, J., (2003). Temporal and cellular requirements for Fms signal indusing zebrafish adult pigment pattern development. *Development* **130**, 817-833.
13. Nakamasu, A., Takahashi, G., Kanbe, A. and Kondo, S., (2009). Interactions between zebrafish pigment cells responsible for the generation of Turing patterns. *Proc Natl. Acad. Sci. U. S. A.* **106**, 8429-8434.
14. Meinhardt, H. and Gierer, A., (1974). Application of a theory of biological pattern

formation based on lateral inhibition. J. Cell Sci. **15**, 132-146.
15. Gierer, A. and Meinhardt, H., (1972). A theory of biological pattern formation. *Kybernetics* **12**, 30-39.
16. Murray J. D., (1989). Mathmatical Biology II. University of Washington, Seattle, WA.
17. Hamada, H., Watanabe, M., Lau, H. E., Nishida, T., Hasegawa, T., Parichy, D. M. and Kondo, S., (2014). Involvement of Delta/Notch signaling in zebrafish adult pigment stripe patterning. *Development* **141**, 318-324.
18. Watanabe, M. and Kondo, S., (2015). Fish pigmentation. Comment on "Local reorganization of xanthophores fine-tunes and colors the striped pattern of zebrafish". *Science* **348**, 297.
19. Kondo, S., (2017). An updated kernel-based Turing model for studying the mechanism of biological pattern formation. *J. Theor. Biol.* **414**, 120-127.
20. Bullara, D. W. and De Decker, Y., (2015). Pigment cell movement is not required for generation of Turing patterns in zebrafish skin. *Nat. Commun.* **6**, 6971.
21. Volkening, A. and Sandstede, A., (2018). Iridophore as a source of robustness in zebrafish stripes and variability in *Danio* patterns. *Nat. Commun.* **9**, 3231.
22. Owen, J. P., Kelsh, R. N. and Yates, C. A., (2020). A quantitative modeling approach to zebrafish pigment pattern formation. *Elife* **9**, E52998.
23. Asai, R. and Kondo, S., (1999). Zebrafish *Leopard* gene as a component of the putative reaction-diffusion system. *Mech. Dev.* **89**, 87-92.
24. Watanabe, M. and Kondo, S., (2012). Chenging clothes easily: connexin41.8 regulates skin pattern variation. *Pigment Cell and Melanoma Res.* 25, 326-330.
25. Takahashi, G. and Kondo, S., (2008). Melanophore in the stripe od adult zebrafish do not have the nature to ather, but disperse when they have the space to move. *Pigment Cell and Melanoma Res.* **21**, 677-686.
26. Sawada, R., Aramaki, T. and Kondo, S., (2018). Flexibility of pigment cell behavior permits the robustness of skin pattern formation. *Genes. Cells* **23**, 537-545.
27. Hirata, M., Nakamura, K., Kanemaru, T., Shibata, Y. and Kondo, S., (2003). Pigment cell organization in the hypodermis of zebrafish. *Dev. Dyn.* **227**, 497-503
28. Hirata, M., Nakamura, K. and Kondo, S., (2005). Pigment cell distributions in different tissues of the zebrafish, with special reference to the striped pigment pattern. *Dev. Dyn.* **234**, 293-300.
29. Mahalwar, P., Walderich, B., Singh, A. P. and Nusslein-Volhard, C., (2014). Local reorganization of xanthophores fine-tunes and colors the striped pattern of zebrafish. *Science* **345**, 1362-1364.
30. Misu, A., Yamanaka, H., Aramaki, T., Kondo, S., Skerrett, I. M., Iovine, M. K. and

Watanabe, M., (2016). Two different functions of connexin43 confer two different bone phenotypes in zebrafish. *J. Biol. Chem.* **291**, 12601-12611.

31. Yamanaka, H. and Kondo, S., (2013). In vitro analysis suggests that difference in cell movement during direct interaction can generate various pigment patterns in vivo. *Proc Natl. Acad. Sci. U. S. A.* **111**, 1867-1872.
32. Ermentrout, B., (1991). Stripes or spots? Nonlinear effects in bifurcation of reaction-diffusion equations on the square. *Proc. R. Soc. A* **434**, 1891.
33. Shoji, H., Iwasa, Y. and Kondo, S., (2003). Stripes, spots, or reversed spots in two-dimensional Turing systems. *J. Theor. Biol.* **224**, 339-350.
34. Miura, T. and Maini, P. K., (2004). Speed of pattern appearance in reaction-diffusion models: Implications in the pattern formation of limb bud mesenchyme cells. Bull. Math Biol, 66(4):627-649.
35. Meinhardt, H., (1982). Chapter 11. Cell determination. In *Models of Biological Pattern Formation.* London; Academic Press.
36. Watanabe, M., Sawada, R., Aramaki, T., Skerrett, I. M. and Kondo, S., (2016). The physiological characterization of connexin41.8 and connexin39.4, which are involved in the striped pattern formation of Zebrafish. *J. Boil. Chem.* **291**, 1053-1063.
37. Watanabe, M., (2017). Gap Junction in the Teleost Fish Lineage: Duplicated Connexins May Contribute to Skin Pattern Formation and Body Shape Determination. *Front. Cell Dev. Boil.* **5**, 13.
38. Inaba, M., Yamanaka, H. and Kondo, S., (2012). Pigment Pattern Formation by Contact-Dependent Depolarization. *Science* **335**, 677.
39. Inaba, M., Jiang, T.-X., Liang, Y.-C., Tsai, S., Lai, Y.-C., Widelitz, R. B. and Chuong, C. M., (2019). Instructive role of melanocytes during pigment pattern formation of the avian skin. *Proc Natl. Acad. Sci. U. S. A.* **116**, 6884-6890.
40. Miyazawa, S., Okamoto, M. and Kondo, S., (2010). Blending of animal colour patterns by hybridization. *Nat. commun.* **1071**, 1-6.

Acknowledgments

The author would like to thank Masakatsu Watanabe and Masafumi Inaba for ~~persistent~~ stimulating discussions and important comments, as well as members of the Higaki lab. for providing a suitable environment to concentrate on this investigation. I would also like to thank Editage (www.editage.com) for English language editing and the IROAST Proofreading/ Publication Support Program. This research was supported from Grant-in-Aid for Scientific Research on Innovative Areas (The Japan Society for the Promotion of Science), Periodicity and its modulation in plant No.20H05421 and Research grant from Shimadzu Science Foundation.

Author contributions

A.N. contributed all of this manuscript.

Competing interests

No competing interests declared

Materials and correspondence

No.

Figures and Tables

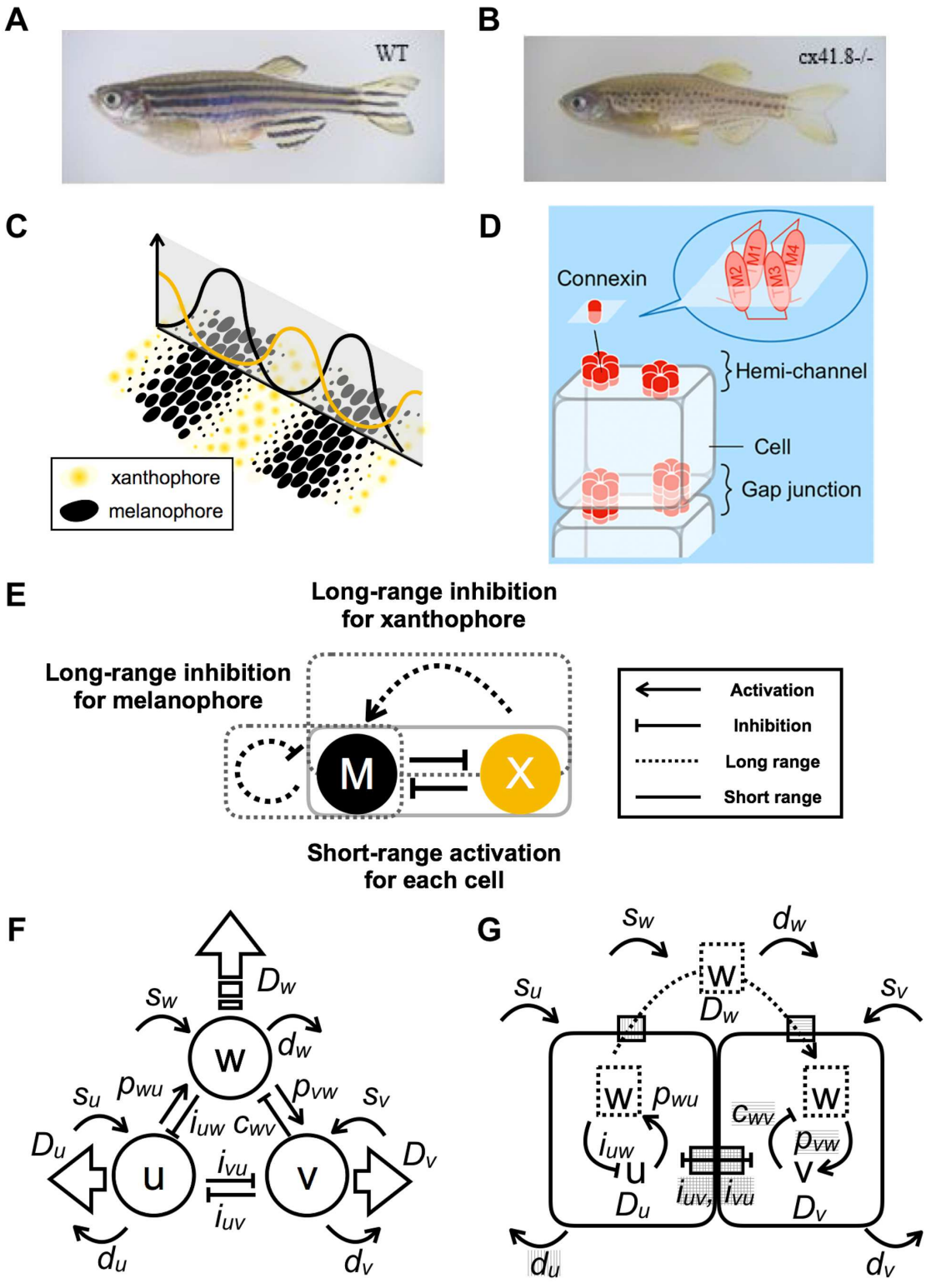

Figure 1. Model-based prediction of defects in channels and interactions.

(A) Striped wild-type (WT) zebrafish. (B) Spotted *leopard* mutant zebrafish. (C) Schematic representation of the relationship between the distribution of pigment cells and the numerical result of the continuous model. (D) Schematic representation of channels composed of connexin complexes. Hemi-channels open to the outside of a cell, whereas gap junctions formed by the docking of hemi-channel connect adjacent cells. (E) Apparent interactions of pigment cells, as revealed by laser ablation experiments. (F) Schematic diagram of a three-variable partial differential equation model composed of components U or V, which correspond to melanophores or xanthophores, respectively, and component w, which represents a highly diffusible molecule. Interactions are indicated by fine arrows, diffusion coefficients (the motility of the components) are indicated by wide arrows, and corresponding parameters are indicated. (G) Schematic diagram of the effect of channels on pigment cells according to the mathematical model. Parameters related to the function of each gate are indicated by hatchings.

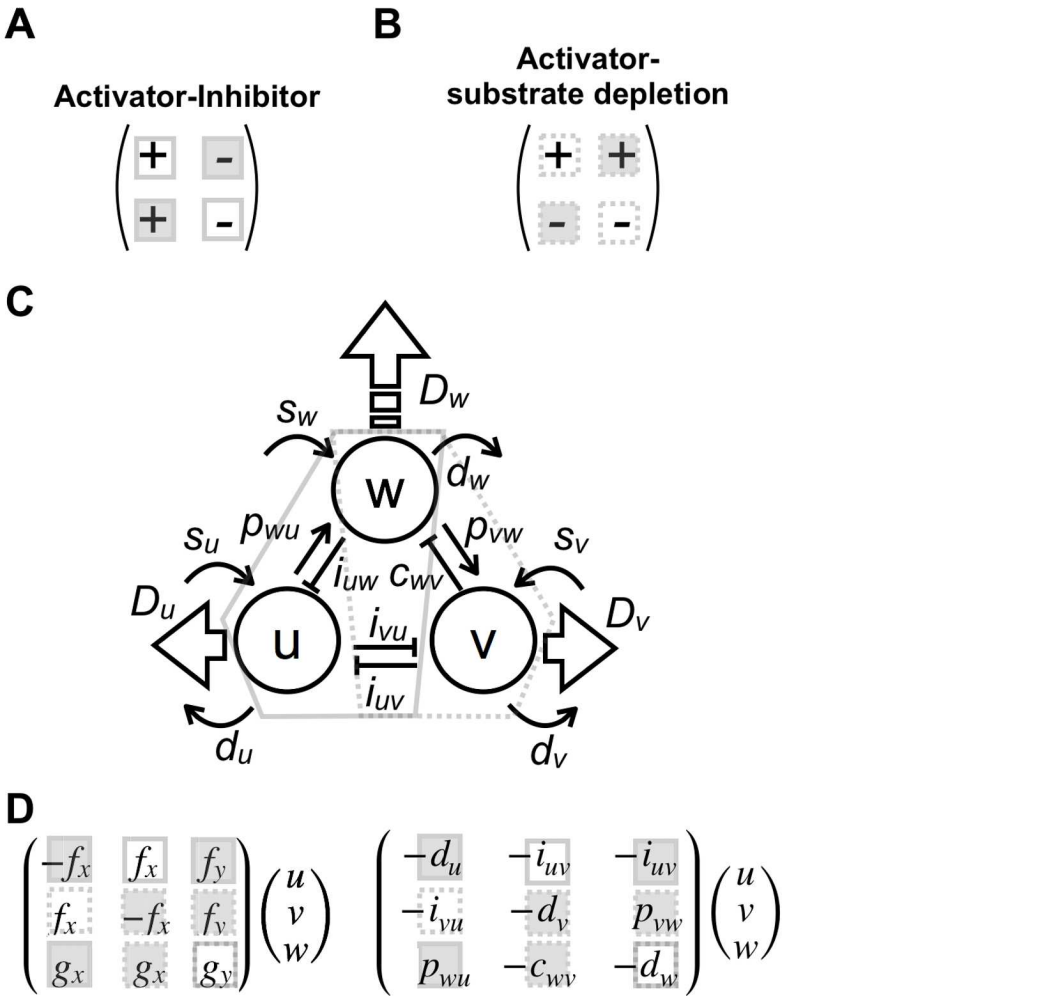

Fig. 2 Parameter correspondences to two-variable systems and effects on pattern size.

(A, B) Two conditions that generate a Turing pattern, activator-inhibitor type (A) or activator-substrate-depletion type (B), with different signs of reaction parameters. (C) Correspondence between parameters in the present tree-component model and the two-variable systems. Interactions included in conditions (A) and (B) are enclosed by solid and dashed polygons, respectively. (D) Matrix forms of reaction terms corresponding to the two-variable system: the filled squares indicate the parameter that increases pattern size when the absolute value is decreased, and the open squares denote the opposite; the solid squares correspond to condition (A), and the dashed ones correspond to condition (B).

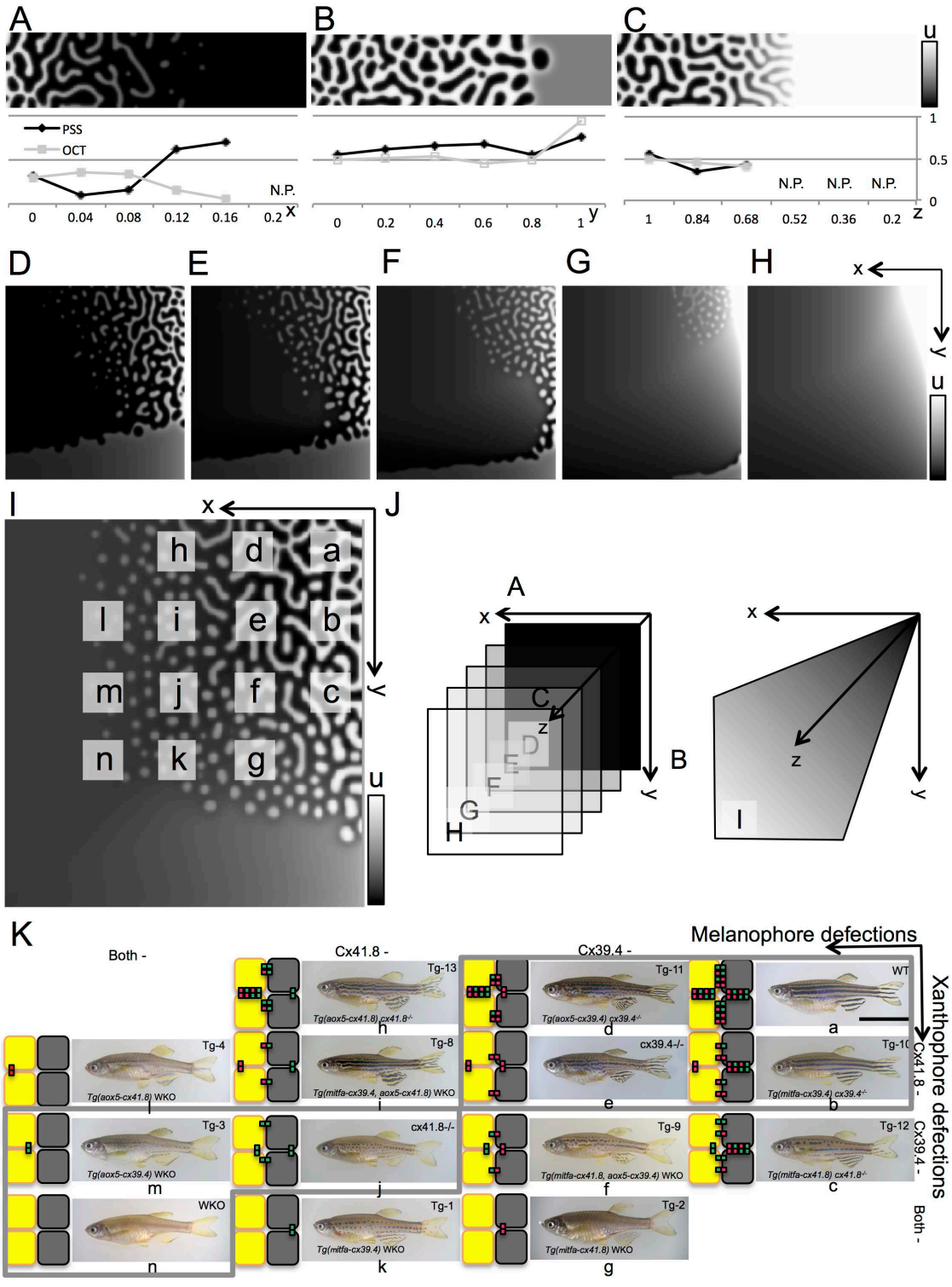

Figure 3 Numerical results of gate effects and comparison with experiments

(A)-(I) Numerical results obtained from a model of linear reaction terms with limits. Pattern shifts were observed when the effects of gate defects on both cells were changed. defects of gates on

U and V cells, and between the cells, become larger along the x- and, y-, and z (or x, y)-axes, respectively. (A)-(C) each defect was analyzed independently with quantification of patterns. (A) *U* defect, (B) V defect, and (C) short-range defects. Pattern simplicity scores (PPS) and overall color tones (OCT) were obtained quantitatively. The short-range effects by gap-junctions were eliminated from arbitral wild-type condition(D) 0.05 to (E) 0.04, (F) 0.03, (G) 0.02, and (H) 0.01. (I) Numerical result of linear terms with limits in which the short-range effects were spontaneously changed along the x- and y-axes with increasing u_d and decreasing v_d. Each small letter indicates the corresponding fish with connexin conditions. (J) Schematics of this analyses utilizing the present linear model. *U* defect, (B) V defect, and (C) short-range defects were changed along with the axes in each panel, as shown in the figures. (K) Pigmentation pattern on connexin-manipulated fish from Usui *et al.*, 2019. Gray flamed fish had correspondence to numerical results.

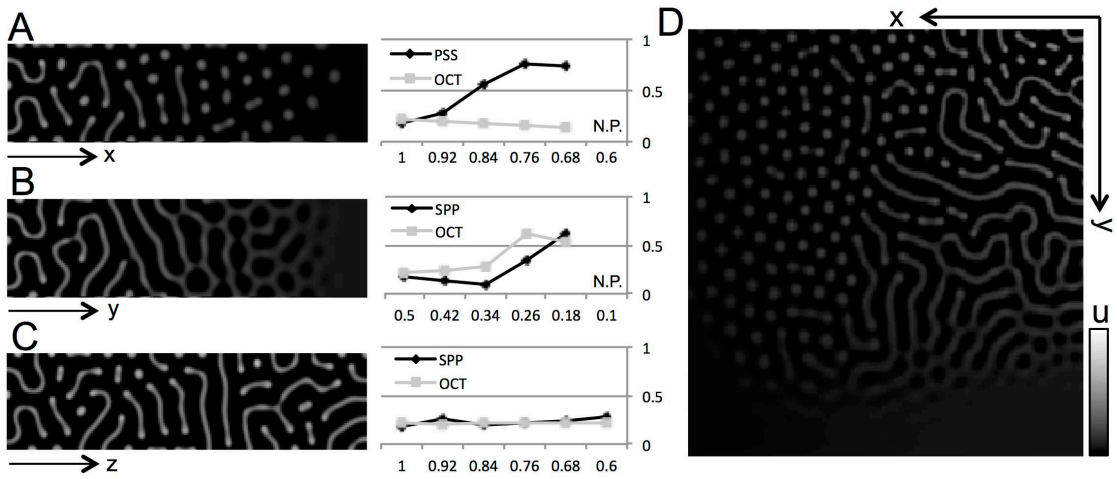

Figure 4 Numerical results of gate effects by nonlinear model

(A-D) Numerical results obtained from a model with nonlinear reaction terms. Pattern shifts were observed when the effects of gate defects on both cells were changed. (A) *U* defect, (B) V defect, and (C) short-range defects, and between the cells, became larger along the x-, y-axes, and z (or x, y)- axes, respectively. Pattern quantification by PSS and OCT are shown on the right. Then the short-range inhibitions were decreased along both axes, spontaneously. All results are shown as density plots of u.

Table 1. Parameter set utilized in this paper.

	D_u, D_v	$-d_u$	$-i_{uv}$	$-i_{uw}$	s_u	$-i_{vu}$	$-d_v$	p_{vw}	s_v	D_w	p_{wu}	$-c_{wv}$	$-d_w$	s_w	min-max (for f, g)	min-max (for h)
Fig.4A	.01	.01	.05	.05	.05	.05	.01	.05	0	1	.05	.07	.05	.02	.0 -.01	.0 -.05
Fig.4B	.01	.01	.04	.05	.05	.04	.01	.05	0	1	.05	.07	.05	.02	.0 -.01	.0 -.05
Fig.4C	.01	.01	.03	.05	.05	.03	.01	.05	0	1	.05	.07	.05	.02	.0 -.01	.0 -.05
Fig.4D	.01	.01	.02	.05	.05	.02	.01	.05	0	1	.05	.07	.05	.02	.0 -.01	.0 -.05
Fig.4E	.01	.01	.01	.05	.05	.01	.01	.05	0	1	.05	.07	.05	.02	.0 -.01	.0 -.05
Fig.S1	.01	.01	.05	.05	.05	.05	.01	.05	0	1	.05	.05	.05	.02	.0 -.01	.0 -.05
Fig.4H-J	.01	-1.	1.	1.	.2	1.	.1	1.	.5	1	1	1.	1.	.0	-	-

Supplemental

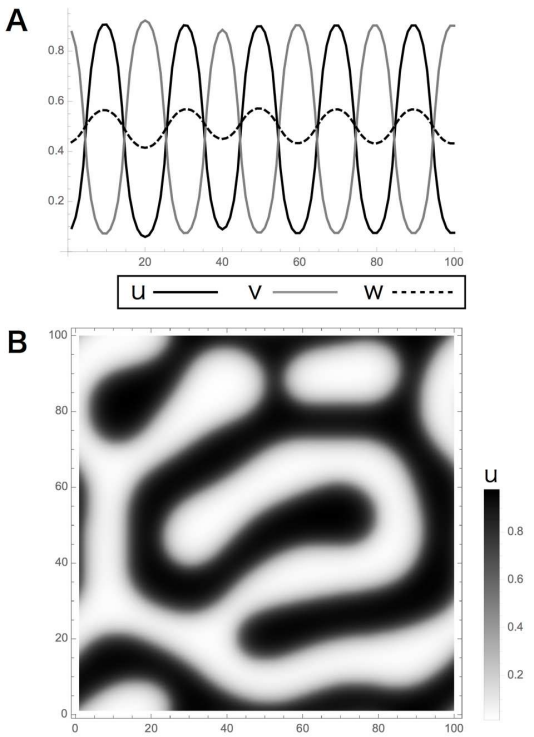

Fig. S1 Turing pattern obtained by applying a reaction-diffusion model.

(A), (B) Calculation results of the model had linear terms with limits. (A) One dimension and (B) two dimensions. Results indicate Turing patterns, in which the variables u and v are distributed complementarily and the highly diffusible molecule W peaks at high u.

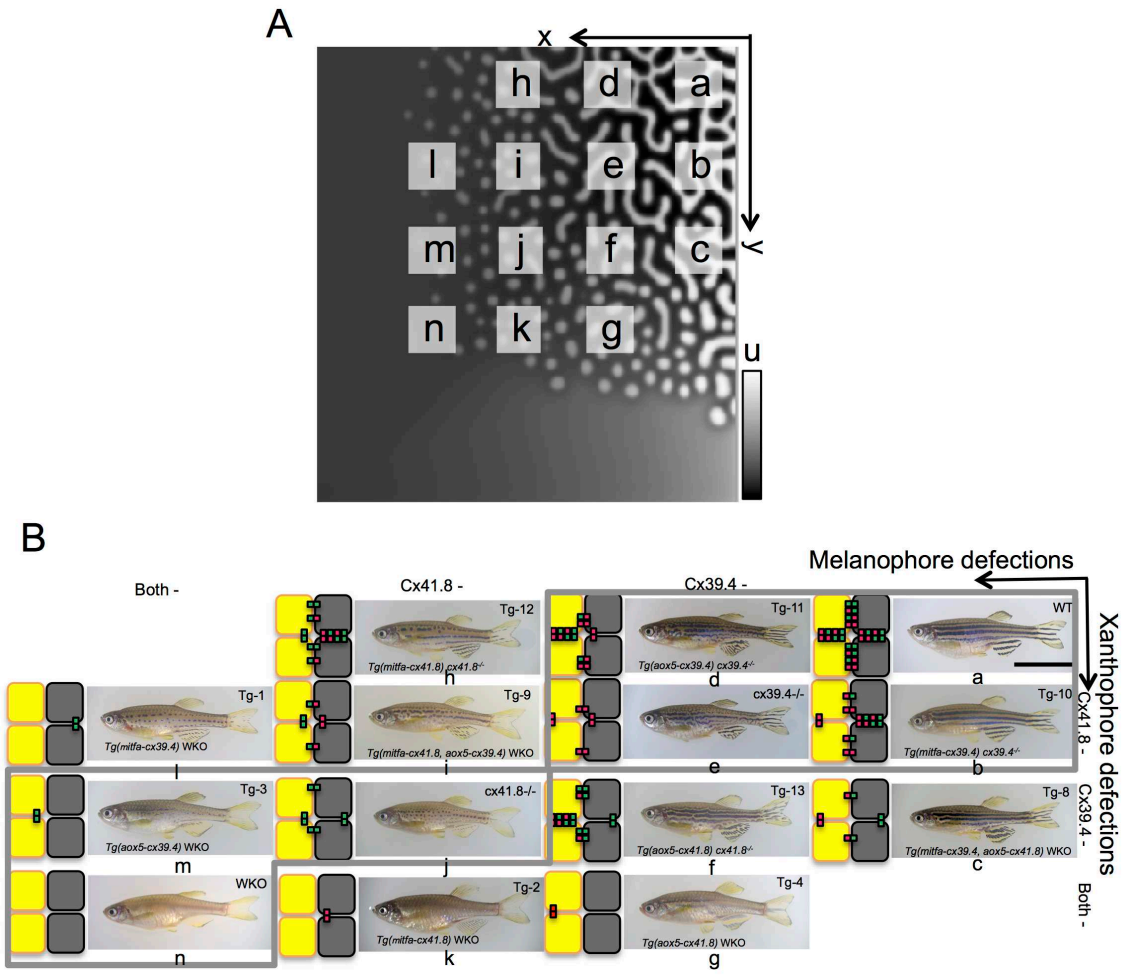

Fig. S2 Shuffle of mutant fish which gives accordance with numerical results.

(A) Density plot of u in calculation results that same as Fig. 3G. The model had linear terms with limits in which the short-range effects were spontaneously changed along the x- and y-axes with defects in gates on u and v cells, respectively. (B) Mutant fish were shuffled for accordance with numerical results. Each small letter indicates the corresponding fish with simulation in the aspect of pattern selection.

Graphical abstract

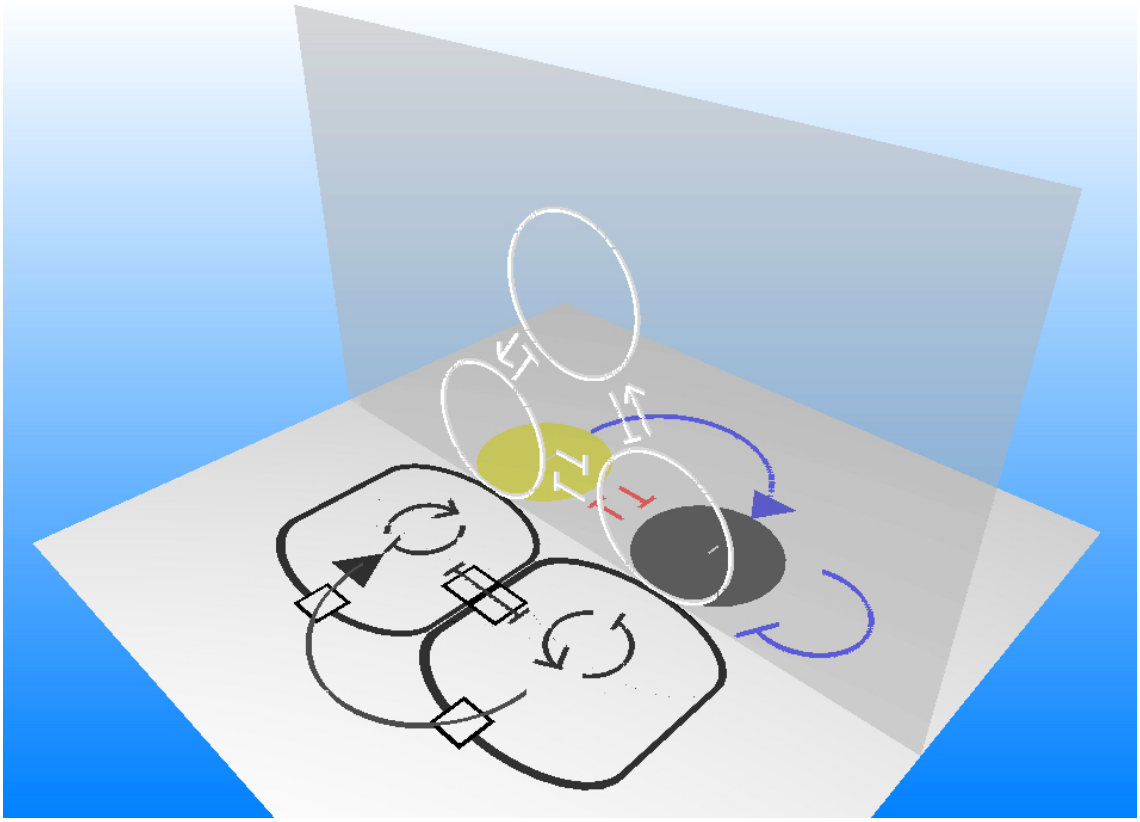

Previously, a three-component reaction-diffusion model (middle, perpendicular panel) was proposed to explain interactions between pigment cells (right back) derived from laser ablation experiments in zebrafish. The model could then be applied to experimental results subsequently obtained after its original development. Interactions in the mathematical model were interpreted on a molecular level and connected with the functions of molecular channels on different cells (left front).